Monthly Notices
of the
ROYAL ASTRONOMICAL SOCIETY

MNRAS **479,** 1401–1411 (2018)
Advance Access publication 2018 June 11

doi:10.1093/mnras/sty1524

ExoMol line lists XXVIII: the rovibronic spectrum of AlH

Sergei N. Yurchenko, Henry Williams, Paul C. Leyland, Lorenzo Lodi and Jonathan Tennyson★

Department of Physics and Astronomy, University College London, London WC1E 6BT, UK

Accepted 2018 June 6. Received 2018 May 19; in original form 2018 April 3

ABSTRACT

A new line list for AlH is produced. The WYLLoT line list spans two electronic states $X\,^1\Sigma^+$ and $A\,^1\Pi$. A diabatic model is used to model the shallow potential energy curve of the $A\,^1\Pi$ state, which has a strong pre-dissociative character with only two bound vibrational states. Both potential energy curves are empirical and were obtained by fitting to experimentally derived energies of the $X\,^1\Sigma^+$ and $A\,^1\Pi$ electronic states using the diatomic nuclear motion codes DPOTFIT and DUO. High-temperature line lists plus partition functions and lifetimes for three isotopologues ^{27}AlH, ^{27}AlD, and ^{26}AlH were generated using *ab initio* dipole moments. The line lists cover both the *X*–*X* and *A*–*X* systems and are made available in electronic form at the CDS and EXOMOL data bases.

Key words: molecular data – opacity – astronomical data bases: miscellaneous – planets and satellites: atmospheres – stars: low-mass.

1 INTRODUCTION

Aluminium is one of the commoner interstellar metallic elements, with a cosmic abundance of Al/H = 3×10^{-6} but AlH has only been rather sparingly observed. AlH was detected in the photospheres of χ Cygni, a Mira-variable S-star, by Herbig (1956) and much more recently around Mira-variable o Ceti by Kaminski et al. (2016). AlH was also detected in sunspots through lines in its $A\,^1\Pi - X\,^1\Sigma^+$ electronic band, which lies in the blue region of the visible (Wallace, Hinkle & Livingston 2000); this spectrum was recently analysed for its rotational temperature by Karthikeyan, Rajamanickam & Bagare (2010).

AlH is difficult to detect in the interstellar medium because of its small reduced mass, which causes its rotational transitions to occur in the submillimetre region. This spectral region is typically filtered by terrestrial atmospheric effects, therefore making it difficult to detect from ground-based observations. So far searches for interstellar AlH have proved negative with, for example, only an upper limit set for the molecule rich IRC+10216 (Cernicharo et al. 2010) using the Herschel Space Observatory. Halfen & Ziurys (2010, 2014, 2016) have undertaken systematic improvement of the AlH submillimetre frequencies, including hyperfine splittings, to aid future detections. The work of Halfen & Ziurys is directly complementary to the work presented here which is aimed at providing ro-vibrational and rovibronic spectroscopic data. Other laboratory studies of AlH spectra, both experimental and theoretical, are discussed below.

Molecular spectra are useful for providing isotopic abundances. Aluminium has only one stable isotope, ^{27}Al, but ^{26}Al has a long half-life, in excess of 700 000 yr. The mass fraction ratio of interstellar ^{27}Al to ^{26}Al can therefore provide important information on the formation of Al isotopes (Mahoney et al. 1984; Diehl et al. 2003; Lugaro et al. 2012); these could be probed using the spectrum of AlH. The AlH molecule is also thought to be an important constituent of the atmospheres of so-called Lava-planets (Tennyson & Yurchenko 2017).

The *A*–*X* band has also been considered as a possible means of producing ultra-cold AlH using laser cooling (Wells & Lane 2011). Lifetimes of the $A\,^1\Pi$ state were measured by Baltayan & Nedelec (1979), while Tao et al. (2003) considered lifetimes for the triplet system *b*–*a*.

Bauschlicher & Langhoff (1988) used a full configuration interaction (FCI) *ab initio* method to produce *ab initio* potential energy and dipole moment curves of AlH, where they also estimated the dissociation energies of the $X\,^1\Sigma^+$ and $A\,^1\Pi$ states and lifetimes of the two bound vibrational sates of $A\,^1\Pi$. The heat of formation of AlH was estimated by Cobos (2002) using DFT methods. Cave, Johnson & Anderson (1994) presented *ab initio* estimates for the dipole moments and transition dipole moments of AlH using a quasi-degenerate variational perturbation theory and averaged coupled-pair functional theory.

The EXOMOL project (Tennyson & Yurchenko 2012) aims to provide line lists of spectroscopic transitions for key molecular species which are likely to be important in the atmospheres of extrasolar planets and cool stars. Rajpurohit et al. (2013) analysed BT-Settl synthetic spectra (Allard 2014) for M-dwarf stars and suggested that the CaOH band at 5570 Å, and AlH and NaH hydrides in the blue

★ Email: j.tennyson@ucl.ac.uk

MNRAS 479, 1401–1411 (2018)

Table 1. Summary of high-resolution spectroscopic data for AlH. FT = Fourier Transform.

Reference	Bands	Method	range in J/v	Frequency range	Comments
Huron (1969)	$A\,^1\Pi - X\,^1\Sigma^+$	Absorption spectroscopy	$v' = 0$–1, $v'' = 0$–4.		
Rafi, Baig & Khan (1978)	$b\,^3\Sigma^+ - a\,^3\Pi$	Emission spectroscopy	$J = 3$–16, $v' = 1$, $v'' = 1$	1–1 band at 3808 Å	3 P-branches, 3 R-branches, unresolved Q
Baltayan & Nedelec (1979)	$A\,^1\Pi - X\,^1\Sigma^+$	Dye laser excitation	$v' = 0$–1, $J = 6$–26		
Deutsch, Neil & Ramsay (1987)	$X\,^1\Sigma^+$, $\Delta v = 2$	Furnace emission	$v = 0$–8, $J = 1$–34		
Zhang & Stuke (1988)	$C\,^1\Sigma^+ - X\,^1\Sigma^+$ $D\,^1\Sigma^+ - X\,^1\Sigma^+$	Dye laser spectrocopy	v', $v'' = 0$,1		
Urban & Jones (1992)	$X\,^1\Sigma^+$, $\Delta v = 1$	Infrared diode laser	$v = 0 - 7$		AlD
Rice, Pasternack & Nelson (1992)	$A\,^1\Pi - X\,^1\Sigma^+$	Emission spectra	$v' = 0$, 1, $v'' = 0$–2	13–30 nm	
Yamada & Hirota (1992)	$X\,^1\Sigma^+$, $\Delta v = 1$	Infrared diode laser	$v = 0$–7, $J = 2$–31		AlH & AlD
Zhu, Shehadeh & Grant (1992)	$C\,^1\Sigma^+ - X\,^1\Sigma^+$ $b\,^3\Sigma^- - X\,^1\Sigma^+$	laser spectrocopy	$v' = 0$–1, $v'' = 0$, $J = 0$–18		
White, Dulick & Bernath (1993)	$X\,^1\Sigma^+$, $\Delta v = 1$	Infrared emission	$v = 0$–7		
Ito et al. (1994)	$X\,^1\Sigma^+$, $\Delta v = 1$	Infrared emission	$v = 0$–3, $J = 0$–22	1400–1800 cm^{-1}	
Goto & Saito (1995)	$X\,^1\Sigma^+$, rotations	Submillimeter	$J = 0$–1	387 GHz	hyperfine resolved
Ram & Bernath (1996)	$A\,^1\Pi - X\,^1\Sigma^+$	FT emission	$v' = 0$–1, $v'' = 0$–4, $J = 0$–18		
Yang & Dagdigian (1998)	$A\,^1\Pi - X\,^1\Sigma^+$	Laser fluorescence	$v = 0$–4		
Nizamov & Dagdigian (2000)	$A\,^1\Pi - X\,^1\Sigma^+$	Fluorescence emission	$v' = 0$, $J = 4$–14		e & f doublets resolved.
Tao et al. (2003)	$b\,^3\Sigma^- - a\,^3\Pi$	Laser fluorescence	$v' = 0$–1, $J = 0$–6	26222–26400 cm^{-1}	$J = 1$ lifetime measured
Halfen & Ziurys (2004)	rotations	Microwave FT	$J = 0$–2	377–393 GHz	hyperfine resolved
Szajna & Zachwieja (2009)	$A\,^1\Pi - X\,^1\Sigma^+$		$v = 0$–3	18 000–25 000 cm^{-1}	$v' = 0$, 1, $v'' = 0$–3, $J = 5$ state perturbed
Halfen & Ziurys (2010)	rotations	Direct absorption	$J = 0$–4	393-590 GHz	AlD
Szajna & Zachwieja (2010)	$C\,^1\Sigma^+ - X\,^1\Sigma^+$		$v' = 0$, 1, $v'' = 0$–2, $J = 0$–28	42000–45000 cm^{-1}	
Szajna et al. (2011)	$C\,^1\Sigma^+ - A\,^1\Pi$ $A\,^1\Pi - X\,^1\Sigma^+$		(0,0), $J = 0$–17(1,1), $J = 0$–7 (0,2), $J = 0$–18	20000–21500 cm^{-1}	
Halfen & Ziurys (2014)	rotations	Direct absorption	$J = 1$–4	755–787GHz	AlH & AlD
Szajna et al. (2015)	$A\,^1\Pi - X\,^1\Sigma^+$	Optical dispersion	(0,0), $J = 0$–29; (1,1), $J = 0$–20; $v = 0$, 1, $J = 0$–29	22400 – 23,700 cm^{-1}	AlD
Szajna et al. (2017)	$A\,^1\Pi - X\,^1\Sigma^+$,$C\,^1\Sigma^+ - A\,^1\Pi$	FT emission	$v' = 0$, 1, $v'' = 0$–3, $J = 0$–29	22400–23,700 cm^{-1}	AlD

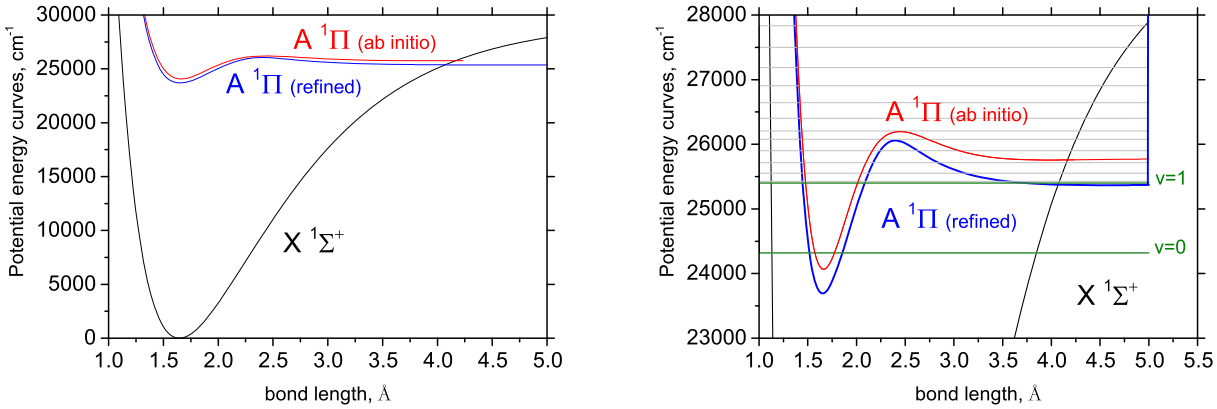

Figure 1. AlH $X\,^1\Sigma^+$ and $A\,^1\Pi$ state potential energy curves. The zoomed figure (right) also shows the AlH vibrational states and DUO vibrational basis functions, see text for details.

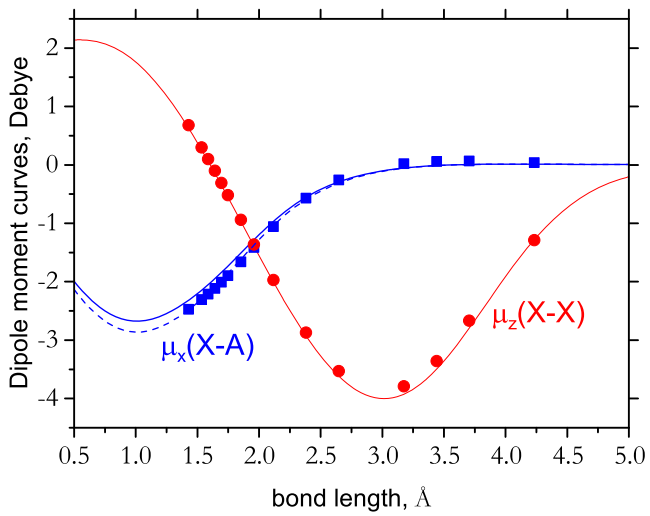

Figure 2. *Ab initio* (transition) dipole moment curves for AlH, *X*–*X*, and *A*–*X*: The solid lines are from this work and the symbols represent the dipoles of Bauschlicher & Langhoff (1988); the dashed curve is a scaled version of our *ab initio* transtion dipole, see text for details.

part of the spectra constituted the main species still missing in the models. An EXOMOL line list for NaH was subsequently computed by Rivlin et al. (2015); here we construct the corresponding line lists for isotopologues ^{27}AlH, ^{27}AlD, and ^{26}AlH of aluminium hydride.

We previously provided line lists for isotopologues of AlO (Patrascu, Tennyson & Yurchenko 2015); this work follows closely on the methodology developed for treating this open shell system (Patrascu et al. 2014). Here we consider transitions within the $X\,^1\Sigma^+ - X\,^1\Sigma^+$ and electronic $A\,^1\Pi - X\,^1\Sigma^+$ bands. The $A\,^1\Pi$ potential energy curve (PEC) is very shallow with a strong predissociative character and can accommodate only two vibrational states (Holst & Hulthén 1934) with a small barrier before the dissociation. Here we apply the diatomic code DUO (Yurchenko et al. 2016) to solve the nuclear motion problem for the $X\,^1\Sigma^+$ and $A\,^1\Pi$ coupled electronic states of AlH and to generate a line list for the *X*–*X* and *A*–*X* bands using empirical PECs and high-level *ab initio* (transition) dipole moment curves (DMC). The centrifugal correction due to the Born–Oppenheimer breakdown (BOB) effect is also considered along with an empirical electronic angular momentum coupling between $X\,^1\Sigma^+$ and $A\,^1\Pi$. The empirical PECs were obtained by fitting the corresponding analytical representations to the experimental energies of AlH derived from the measured line positions available in the literature using the MARVEL (measured active rotation-vibration energy levels) methodology (Furtenbacher, Császár & Tennyson 2007). Special measures were taken to ensure that the unbound and quasi-bound states are not included in the line lists. Lifetimes and partition functions are also provided as part of the line lists supplementary material, which are available from the CDS and EXOMOL data bases. Comparisons with experimental spectra and lifetimes are presented.

The paper is structured as follows. Section 2 describes the methods used and includes a discussion of previous laboratory data, Section 3 presents our results and Section 4 offers some conclusions.

2 METHOD

Rotation-vibration resolved lists for the ground $X\,^1\Sigma^+$ and $A\,^1\Pi$ excited electronic states of AlH were obtained by direct solution of the nuclear-motion Schrödinger equation using the DUO program (Yurchenko et al. 2016) in conjunction with empirical PECs and *ab initio* (transition) DMCs. In principle the calculations could be performed using *ab initio* PECs and coupling curves (Tennyson et al. 2016a); however, in practice this does not give accurate enough transition frequencies or wavefunctions so the PECs was actually characterized by fitting to observed spectroscopic data. Conversely, experience (Tennyson 2014) suggests that retaining *ab initio* diagonal and transition dipole moment curves give the best predicted transition intensities; this approach is adopted here.

2.1 Experimental data

There has been considerable laboratory work on the spectrum of AlH and AlD. High-resolution studies considered for this work are summarized in Table 1. In addition there have been a recent studies involving higher electronic states of AlH by Szajna et al. (2017a) and Szajna, Moore & Lane (2017b).

Transition frequencies of AlH were collected from papers by Deutsch et al. (1987); Yamada & Hirota (1992); White et al. (1993); Ito et al. (1994); Ram & Bernath (1996); Halfen & Ziurys (2004); Szajna & Zachwieja (2009); Szajna et al. (2011), and Halfen & Ziurys (2014) listed in Table 1 which concerned ^{27}AlH and ^{27}AlD and transitions within the ground electronic state or the $A\,^1\Pi - X\,^1\Sigma^+$ band. The transitions were used as input for a MARVEL

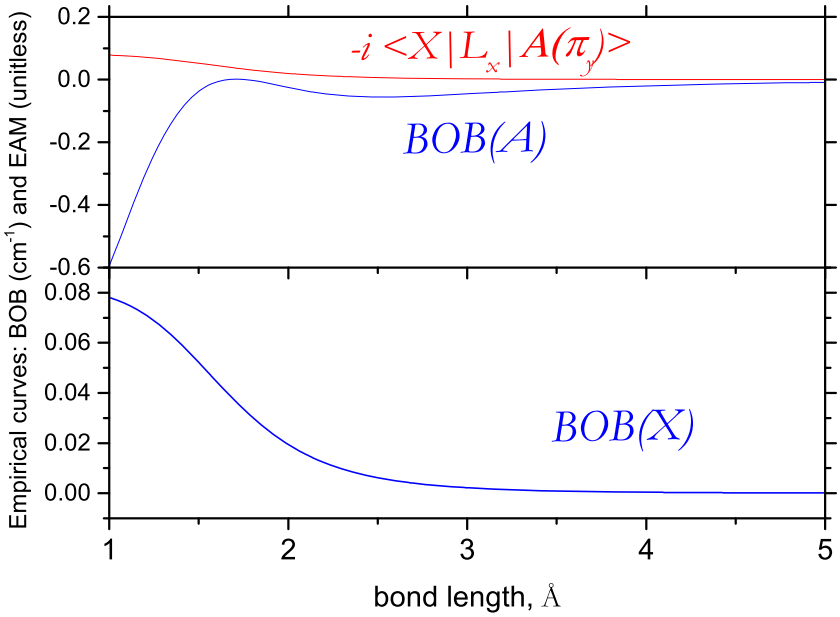

Figure 3. Empirical curves for AlH: BOB for the $X\,^1\Sigma^+$ and $A\,^1\Pi$ states, plus the L_x electronic angular momentum coupling between the two states.

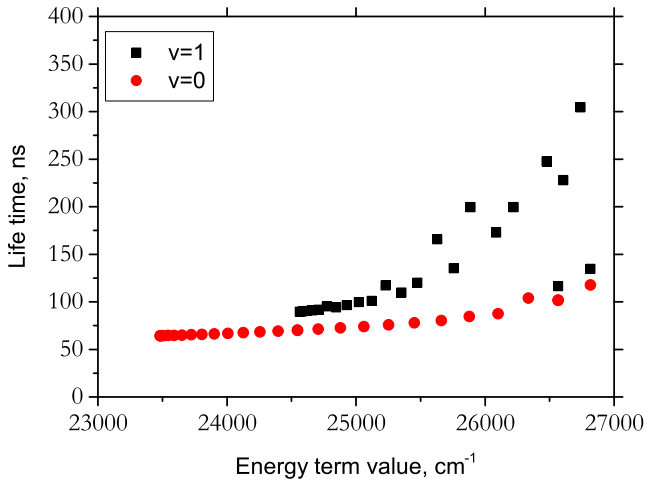

Figure 4. Lifetimes of AlH states in the $A\,^1\Pi$ state.

analysis (Furtenbacher et al. 2007; Furtenbacher & Császár 2012). Much of the data (Yamada & Hirota 1992; Ito et al. 1994; Ram & Bernath 1996; Szajna & Zachwieja 2009; Szajna et al. 2011) was validated by MARVEL requiring, at most, small adjustments of the assigned uncertainties to make them consistent with each other.

The work of Halfen & Ziurys (2004, 2014) is hyperfine-resolved but hyperfine splittings are not present in the other studies and are not considered in this work.

The works of White et al. (1993) and Deutsch et al. (1987) are important as the source of high-v numbers (up to $v = 5$ and $v = 8$, respectively) in the $X\,^1\Sigma^+$ state.

Running MARVEL on this network of 917 validated transitions gave 331 empirical energy levels, 283 in the $X\,^1\Sigma^+$ state, and 48 in the $A\,^1\Pi$ state of ^{27}AlH. For the $X\,^1\Sigma^+$ state, J spanned the range 0 to 40 and v went from 0 to 8. For the $A\,^1\Pi$ state, J spanned the range 0–29 and v only included 0 and 1. Note that the $A\,^1\Pi$ state is very shallow and supports, at most, only these two vibrational states. This issue is discussed further below.

In the case of ^{27}AlD, 581 experimental transition frequencies X–X were taken from Urban & Jones (1992), Yamada & Hirota (1992) and Halfen & Ziurys (2004), and used in MARVEL to produce 301 term values of $X\,^1\Sigma^+$ covering $v = 0$–7 and $J = 0$...39. The A state term values were taken directly from Szajna et al. (2015) ($v = 0$, 1, $J_{\max} = 29$).

2.2 Potential energy and dipole moment curves

There are a number of previous studies of the $A\,^1\Pi$ and $X\,^1\Sigma^+$ curves of AlH, see Brown & Wasylishen (2013), Seck et al. (2014), and references therein. The ground electronic PEC has a nice Morse-like structure. Experimental data on the X state cover vibrational excitations up to $v = 8$; therefore we decided to obtain the X-state PEC fully empirically by fitting it to the experimental frequencies from Deutsch et al. (1987); White et al. 1993; Ito et al. 1994. The X-state PEC was represented using an Extended Morse Oscillator (EMO) potential (Lee et al. 1999) given by

$$V(r) = V_e + (A_e - V_e)\left[1 - \exp\left(-\beta_{\rm EMO}(r)(r - r_e)\right)\right]^2, \quad (1)$$

where $(A_e - V_e)$ is the dissociation energy, V_e is the minimum of the PEC, which for the $X\,^1\Sigma^+$ state was set to zero, r_e is the equilibrium internuclear bond distance, $\beta_{\rm EMO}$ is the distance dependent exponent coefficient, defined as

$$\beta_{\rm EMO}(r) = \sum_{i=0}^{N} B_i \xi_p(r)^i \quad (2)$$

where N is the expansion order parameter, and ξ_p is the SŽurkus variable (Šurkus, Rakauskas & Bolotin 1984) given by

$$\xi_p(r) = \frac{r^p - r_{\rm ref}^p}{r^p + r_{\rm ref}^p} \quad (3)$$

with p as a parameter. Use of the EMO has two advantages. First, it guarantees a correct dissociation limit and second, allows extra flexibility in the degree of the polynomial around a reference position $r_{\rm ref}$, which was defined as the equilibrium internuclear separation

Table 2. Extract from the state file for $^{27}Al^{1}H$. Full tables are available from http://cdsarc.u-strasbg.fr/cgi-bin/VizieR?-source=J/MNRAS/xxx/yy and www.exomol.com.

n	Ë	g_i	J	τ	Parity	e/f	State	v	Λ	Σ	Ω
1	0.000000	12	0	inf	+	e	X1Sigma+	0	0	0	0
2	1625.069321	12	0	4.9283E-03	+	e	X1Sigma+	1	0	0	0
3	3194.213685	12	0	2.6224E-03	+	e	X1Sigma+	2	0	0	0
4	4708.817022	12	0	1.8630E-03	+	e	X1Sigma+	3	0	0	0
5	6170.193041	12	0	1.4908E-03	+	e	X1Sigma+	4	0	0	0
6	7579.564189	12	0	1.2739E-03	+	e	X1Sigma+	5	0	0	0
7	8938.046805	12	0	1.1350E-03	+	e	X1Sigma+	6	0	0	0
8	10246.644027	12	0	1.0410E-03	+	e	X1Sigma+	7	0	0	0
9	11506.245734	12	0	9.7519E-04	+	e	X1Sigma+	8	0	0	0
10	12717.633797	12	0	9.2834E-04	+	e	X1Sigma+	9	0	0	0

Notes: n: State counting number.
$\tilde{E}$: State energy in cm^{-1}.
g_i: Total statistical weight, equal to $g_{ns}(2J + 1)$.
J: Total angular momentum.
τ: Lifetime (s^{-1}).
+/ −: Total parity.
e/f: Rotationless parity.
State: Electronic state.
v: State vibrational quantum number.
Λ: Projection of the electronic angular momentum.
Σ: Projection of the electronic spin.
Ω: Projection of the total angular momentum, $\Omega = \Lambda + \Sigma$.

Table 3. Extracts from the transitions file for ^{27}AlH. Full tables are available from http://cdsarc.u-strasbg.fr/cgi-bin/VizieR?-source=J/MNRAS/xxx/yy and http://www.exomol.co.

F	I	A_{FI}	$\tilde{\nu}_{FI}$
1075	1087	0.5502E-09	47.949528
1529	1488	1.5634E-11	47.965895
561	520	6.1183E-02	47.984746
218	176	0.6544E-09	48.007351
1415	1384	1.4996E-11	48.171601
441	399	1.1015E-01	48.615068
198	156	0.8765E-09	48.846517
198	156	3.0699E-03	48.846517

Notes: F: Upper state counting number;
I: Lower state counting number;
A_{FI}: Einstein A coefficient in s^{-1}.
$\tilde{\nu}_{FI}$: Energy term value in cm^{-1}.

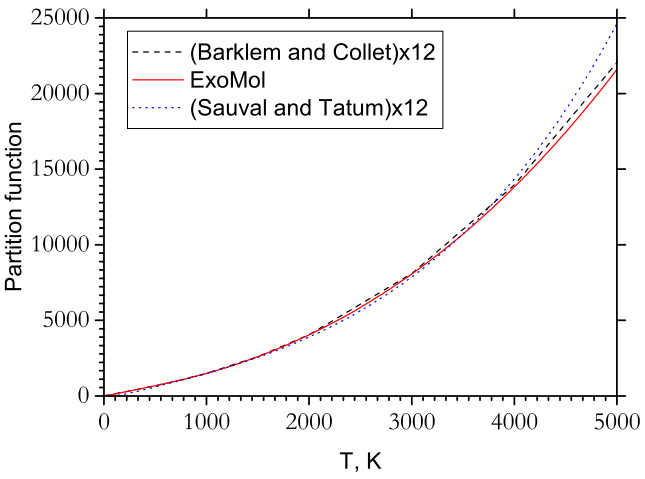

Figure 5. Temperature dependence of the partition function of ^{27}AlH computed using our line lists and compared to those by Sauval & Tatum (1984) and Barklem & Collet (2016).

(r_e) in this case. Fig. 1 shows our empirical PEC of AlH in its X state.

This closed shell $X\,^1\Sigma^+$ ground state was fitted to an EMO using DPOTFIT (Le Roy 2017a). To allow for rotational BOB effects (Le Roy 2007) which become important for $J > 20$, the vibrational kinetic energy operator was extended by

$$-\frac{\hbar^2}{2\mu r^2} \rightarrow -\frac{\hbar^2}{2\mu r^2}\left(1 + g^{\rm BOB}(r)\right), \quad (4)$$

where the unitless BOB functions $g^{\rm BOB}$ are represented by the polynomial

$$g^{\rm BOB}(r) = \left[(1-\xi_p)\sum_{k\geq 0}^{N_T} A_k \xi_p^k + \xi_p A_\infty\right] \quad (5)$$

where ξ_p as the SŽurkus variable and p, A_k and A_∞ are adjustable parameters; in practice we used $A_\infty = 0$.

Given the shallow nature of the A curve which also appears to undergo an avoided crossing we decided to perform our own calculations using a high level of electronic structure theory. *Ab initio* PECs and Dipole Moment Curves (DMCs) were computed using

Table 4. Fitting parameters used to represent the partition functions, see equation (14). Fits are valid for temperatures up to 5000 K.

Parameter	^{27}AlH	^{27}AlD	^{26}AlH
a_0	1.07862304206	1.25534381874	1.34186025327
a_1	0.38191971276	0.22993489470	0.38228272653
a_2	− 2.22562466705	− 1.92470848538	− 2.22605038250
a_3	4.34557816661	6.16172026680	4.34313450679
a_4	− 3.62598781682	− 7.66641279825	− 3.62196458297
a_5	1.71637190159	5.35122144723	1.71374588820
a_6	− 0.47932820561	− 2.24207082067	− 0.47845359880
a_7	0.07359563236	0.55715405704	0.07344763428
a_8	− 0.00476226937	− 0.07543604728	− 0.00475215090
a_9	–	0.00427936817	–

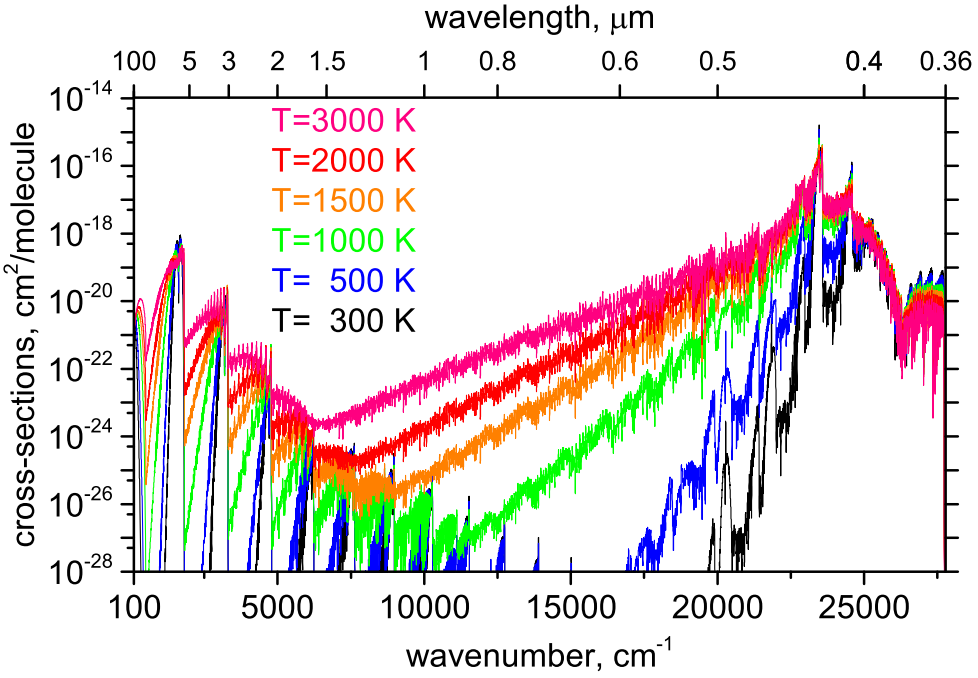

Figure 6. Temperature dependence of the AlH absorption spectrum using the Gaussian profile with HWHM = 5 cm^{-1}. The absorption profile becomes flatter with increasing temperature.

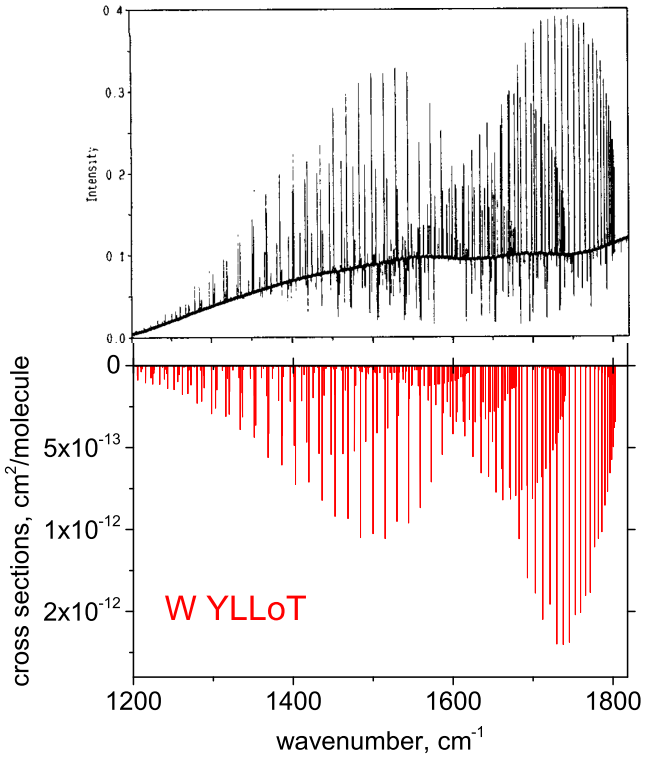

Figure 7. Infrared spectrum of AlH by White et al. (1993) (upper) compared to the emission spectrum computed using our line list assuming a temperature of 1700 K and a Gaussian profile with the HWHM of 0.01 cm^{-1}. Reproduced from White et al. (1993), with the permission of AIP Publishing.

the MOLPRO electronic structure package (Werner et al. 2012) at the multireference configuration interaction (MRCI) level using an aug-cc-pV5Z Gaussian basis set. Calculations were performed at 120 bond lengths over the range of $r = 2$ to 8 a_0. Fig. 1 shows the *ab initio* PEC of $A\,^1\Pi$, which only supports two bound vibrational states. It also shows a maximum at about 4.5 a_0 which is probably associated with an avoided crossing. Fig. 2 shows our *ab initio* DMCs, which agree well with the *ab initio* dipole moment values from Bauschlicher & Langhoff (1988), although, as discussed below, the magnitude of our transition dipole is slightly smaller. Our calculations give a permanent dipole moment of 0.158 D (absolute value) at $r = 1.646$ Å at equilibrium, which is slightly higher than that by Bauschlicher & Langhoff (1988), 0.12 D. This is significantly less than the absolute value of 0.186 used by CDMS (Müller et al. 2005), which is taken from an old calculation by Meyer & Rosmus (1975). We also note that the X dipole also changes sign close to equilibrium. We return to these issues below. Matos et al. (1988) in their *ab initio* work showed a strong variation of the dipole and obtain a value of 0.3 D for μ_0 (i.e. a vibrational averaged in the ground vibrational state), while our value is 0.248 D. No experimental values exist. The $A\,^1\Pi - X\,^1\Sigma^+$ transition dipole moment of AlH also undergoes a change in behaviour in the region around 4.5 a_0.

In order to represent the complex shape of the shallow $A\,^1\Pi$ potential energy curve (see Fig. 1), we used a diabatic-like scheme, where the effect of the avoided crossing is described by a 2 × 2 matrix:

$$\underline{B} = \begin{pmatrix} V_1(r) & W(r) \\ W(r) & V_2(r) \end{pmatrix}. \quad (6)$$

Here $V_1(r)$ is given by the EMO potential function in equation (1), while $V_2(r)$ is represented by a simple repulsive form

$$V_2(r) = \frac{w_6}{r^6}.$$

The coupling $W(r)$ is given by

$$W(r) = W_0 + \frac{\sum_{i\geq 0} w_i (r - r_{\rm cr})^i}{\cosh[\beta(r - r_{\rm cr})]}, \quad (7)$$

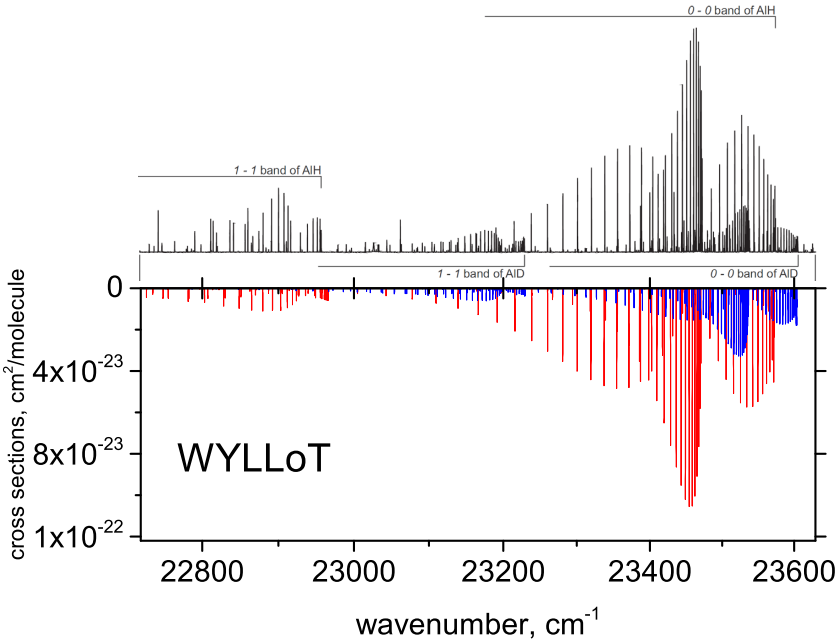

Figure 8. Comparison between the 0–0 and 1–1 bands of the $A\,^1\Pi - X\,^1\Sigma^+$ emission spectrum of AlH and AlD measured by Szajna et al. (2015) (upper) and computed using our line list (lower) assuming a temperature of 4500 K (vibrational) and 900 K (rotational). The intensities of the AlD theoretical spectrum, given in blue and annotated in the experimental spectrum, are scaled by a factor 0.5. Reprinted from Szajna et al. (2015), Copyright (2015), with permission from Elsevier.

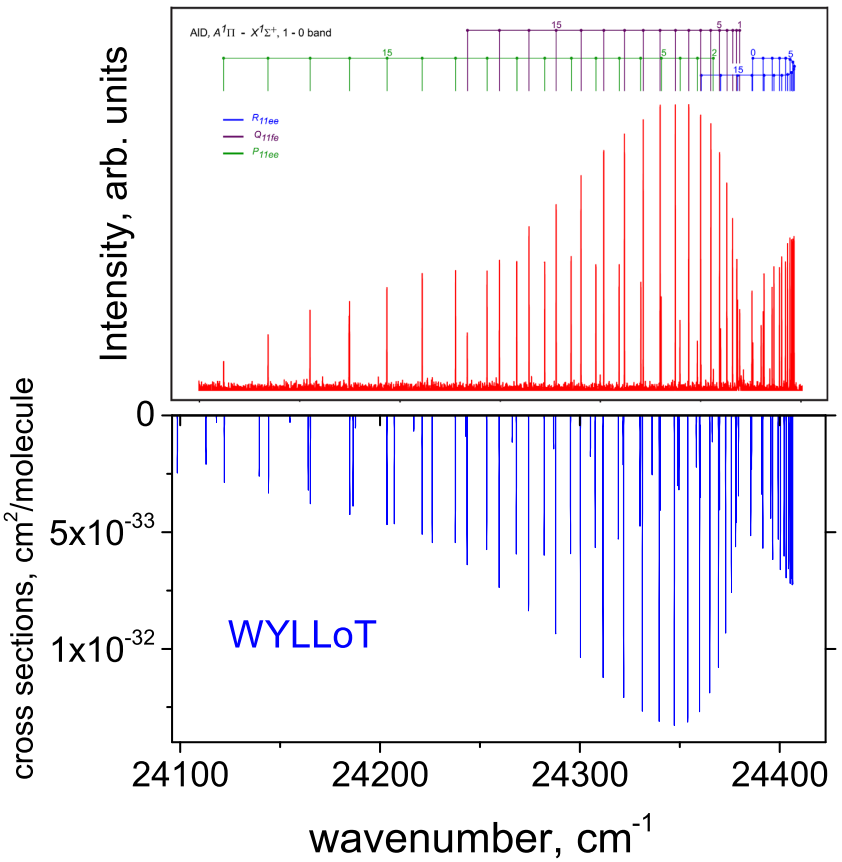

Figure 9. Comparison between the 1–0 band of the $A\,^1\Pi - X\,^1\Sigma^+$ emission spectrum of AlD measured by Szajna et al. (2017) (upper) and computed using our line list assuming a temperature of 600 K. Reprinted from Szajna et al. (2017), Copyright (2017), with permission from Elsevier.

Table 5. $A\,^1\Pi - X\,^1\Sigma^+$ Einstein coefficients $A_{v'v''}$ (s^{-1}) compared to experimentally derived ratios from Rice et al. (1992), where we used $J' = 1$ and $J'' = 0$.

	This work	Exp.
A_{00}	9028000	
A_{01}	3878	
A_{10}	810100	
A_{12}	165900	
A_{11}	5407000	
A_{01}/A_{00}	0.00043	0.0018 ± 0.0001
A_{12}/A_{11}	0.03068	0.029 ± 0.004
A_{10}/A_{11}	0.14982	0.15 ± 0.02

where r_{cr} is a crossing point. The two eigenvalues of $\underline{B}$ are given by

$$V_{low}(r) = \frac{V_1(r) + V_2(r)}{2} - \frac{\sqrt{[V_1(r) - V_2(r)]^2 + 4\,W^2(r)}}{2}, \quad (8)$$

$$V_{upp}(r) = \frac{V_1(r) + V_2(r)}{2} + \frac{\sqrt{[V_1(r) - V_2(r)]^2 + 4\,W^2(r)}}{2}, \quad (9)$$

where the lowest root $V_{low}(r)$ corresponds to the $A\,^1\Pi$ adiabatic PEC.

Initially, the expansion parameters representing this form were obtained by fitting to the *ab initio* *A*-state PEC shown in Fig. 1 and then refined by fitting to the MARVEL energies. Currently DUO does not support quasi-bound or continuum solutions, see Yurchenko et al. (2016). Technically, by virtue of the sinc DVR (discrete variable representation) method used by DUO to solve the vibrational ($J = 0$) Schrödinger equation, DUO uses infinite walls at each end of the integration grid (0.5–5.0 Å in our case) as boundary conditions, which is illustrated in Fig. 1. For the $A\,^1\Pi$ state, we selected 20 basis functions generated by solving the $J = 0$ problem for the PEC of the $A\,^1\Pi$ state using the sinc DVR method (and 60 vibration basis functions for $X\,^1\Sigma^+$). All these basis set functions have zeros at the boundaries, $r = 0.5$ and 5.0 Å, and thus represent bound wavefunctions. Therefore the solution of the coupled rovibronic Schrödinger equations with this basis set contains a mixture of real $A\,^1\Pi$ bound states ($v = 0$ and $v = 1$) and a large number of continuum states. The corresponding energies of these states for $J = 0$ are shown in Fig. 1 as horizontal lines. From these solutions only the $v = 0$ and $v = 1$ states are actually bound and thus selected for the final line list. The bound states can be easily distinguished from the quasi- or unbound states using the *A*–*X* transition probabilities or lifetimes, which differ by 3–4 orders of magnitude. It should be noted that the $A\,^1\Pi$ computed energies suffer from accidental resonances at higher values of *J* between bound and unbound states, which affect the accuracy of the calculated $v = 0$ and $v = 1$ energies. As shown below, this is partly resolved by replacing the theoretical energies with the experimentally derived (MARVEL) values.

The BOB-correction in the form given in equation (5) was used for the *A*-state as well. In these fits the *X*-state parameters were fixed to the values obtained using Level. The BOB-curves are shown in Fig. 3.

In order to account for the Λ-doubling effect, we also used an empirical electronic angular momentum (EAM) coupling between the $A\,^1\Pi$ and $X\,^1\Sigma^+$ states, which was represented by

$$H^{EAM}(R) = (1 - \xi)A_0^{EAM}, \quad (10)$$

which is nothing else than equation (5) truncated after the leading term. The final value of A_0^{EAM} is 0.1475 cm^{-1} and the EAM curve is shown in Fig. 3.

The final fit gave an observed minus calculated root-mean-square (rms) error of 0.025 cm^{-1}, when compared to our MARVEL energy levels for the $X\,^1\Sigma^+$ state. The MARVEL energy levels of the $A\,^1\Pi$ state are reproduced with an rms error of 0.59 cm^{-1}.

Baltayan & Nedelec (1979) reported AlH dissociation energies measured using a hollow cathode discharge by dye laser excitation, 3.16 ± 0.01 eV and 0.24 ± 0.01 eV for the $X\,^1\Sigma^+$ and $A\,^1\Pi$ states, respectively. The dissociation energy (D_e) of our empirical PEC of the $X\,^1\Sigma^+$ state is 3.644 eV which overestimates the experimental value. By allowing D_e to vary in our fit, we achieved a more accurate and stable fit for the lower part of the PEC ($v = 0, \ldots, 8$), which however leads to a D_e value higher by about 0.5 eV than the empirical value of Baltayan & Nedelec (1979). The upper part of the PEC is less important for astrophysical applications, and is also commonly perturbed by contributions from upper electronic states not considered in out fit. Therefore our usual approach is to sacrifice the accuracy of D_e for the sake of a better representation of the lower lying vibrational states. This should not be a problem for our AlH line lists since the contribution to the various spectra considered below from the $X\,^1\Sigma^+$ state highly excited vibrational states is negligible. For the $A\,^1\Pi$ PEC we obtained $D_e = 0.209$ eV (*ab initio*) and 0.210 eV (refined PEC), which compare well to the experimental value of Baltayan & Nedelec (1979). It should be noted that Bauschlicher & Langhoff (1988) also reported *ab initio* FCI dissociation energies which coincide with the experimental values of Baltayan & Nedelec (1979).

Since the current version of DUO does not account for the isotopic-effect explicitly and thus is not capable of treating a mass-independent model as, for example, in LEVEL Le Roy (2017b), we had to create independent models for different isotopologues. Therefore the same fitting procedure was repeated for AlD, where the model curves were fitted to the AlD experimentally derived energies (MARVEL). Fortunately, the experimental data set for AlD is almost as large as that for AlH.

Final parameters for all the curves representing our two spectroscopic models for AlH and AlD (PECs, DMCs, and other empirical curves) and used in DUO are given in the supplementary material in the form of the DUO input. The program DUO is freely available via the www.exomol.com web site. The actual curves can be extracted from the DUO outputs, which are also provided.

2.3 Lifetimes

The lifetimes of AlH in the $A\,^1\Pi$ state were measured by Baltayan & Nedelec (1979) using a hollow cathode discharge by dye laser excitation, who reported two values: 66 ± 4 ns ($v = 0$, $J = 7$) and 83 ± 6 ($v = 1$, $J = 5$). Using our Einstein coefficients and program EXOCROSS (Yurchenko, Al-Refaie & Tennyson 2018a) we obtained 73.6 ns and 102.5 ns for these states, respectively. These lifetimes can also be compared to theoretical values given by Bauschlicher & Langhoff (1988) of 64.3 ns and 96.6 ns, respectively. Our lifetimes are about 1.14 times longer than experiment, which indicates that the absolute value of our transition dipole moment *A*–*X* is about 1.07 times too small. Considering that the *A*–*X* transition dipole of Bauschlicher & Langhoff (1988) is also the same factor larger, see in Fig. 2, we decided to scale our *ab initio* *A*–*X* transition dipole moment by a factor of 1.07. The resulting transition dipole moment is shown in Fig. 2, where it matches better the *ab initio* TDMC by Bauschlicher & Langhoff (1988). Using the scaled TDMC, we also obtain a better match for the lifetimes: 64.3 ns ($v = 0$, $J = 7$) and 89.6 ($v = 1$, $J = 5$). This transition DMC is used to produce the AlH line lists presented below.

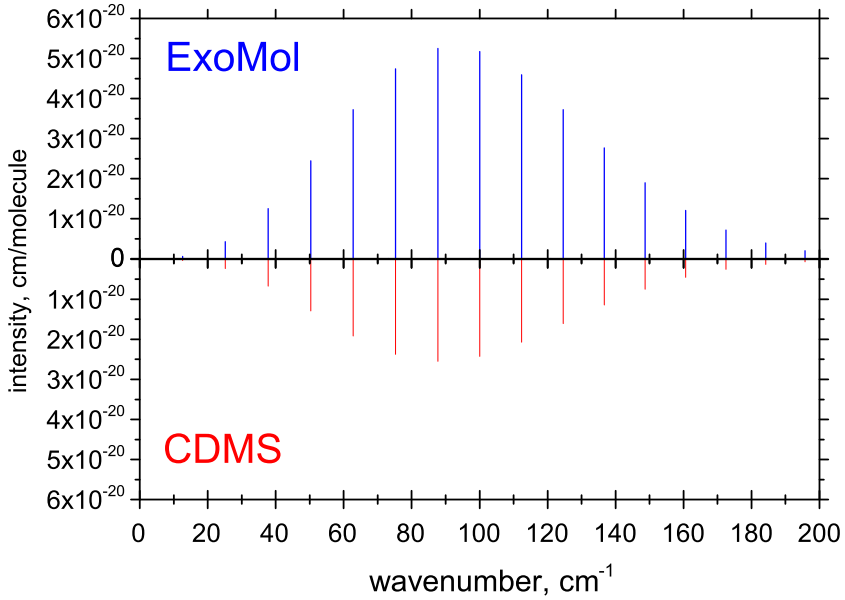

Figure 10. Comparison between pure rotational spectrum of ^{27}AlH at 298 K given by CDMS (Müller et al. 2005) (lower) and computed using our line list (upper).

Fig. 4 shows our lifetimes of the $v = 0$ and $v = 1$ (A) rovibronic states of AlH using the scaled DMC. The oscillations in the $v = 1$ progression is probably due to accidental resonances with unbound states (see below).

2.4 Line list generation

Line lists for AlH and AlD were generated using the program DUO.

To reduce the numerical noise in the intensity calculations of high overtones characterized by small transition probabilities in the spectra of the $X\,^1\Sigma^+$ state (see recent recommendations by Medvedev et al. 2016) the DMCs are represented analytically. We use the following expansion (Prajapat et al. 2017; Yurchenko et al. 2018b):

$$\mu(r) = \sum_{k=0}^{N} \mu_k\, z^k (1 - \xi_p), \tag{11}$$

where z is the damped-coordinate given by:

$$z = (r - r_{\rm ref})\, e^{-\beta_2 (r - r_{\rm ref})^2 - \beta_4 (r - r_{\rm ref})^4}. \tag{12}$$

Here $r_{\rm ref}$ is a reference position equal to $r_{\rm e}$ by default and β_2 and β_4 are damping factors. The expansion parameters are given in the supplementary material. As an additional measure to reduce numerical noise in the overtone intensities, a dipole moment cutoff of 10^{-7} D was applied to the vibrational dipole moments: all transitions for which the vibrational dipole moments are smaller than 10^{-7} D were ignored.

The $A\,^1\Pi - X\,^1\Sigma^+$ (bound) spectrum only contains transitions to/from the upper states $v' = 0$ and $v' = 1$, i.e. no overtones, and thus should not suffer from the numerical noise issue as much as the $X\,^1\Sigma^+ - X\,^1\Sigma^+$ band. Therefore the $A\,^1\Pi$–$X\,^1\Sigma^+$ transition dipole moment was given directly in the (scaled) *ab initio* grid representation of 120 points. The latter points are interpolated by DUO on to the sinc DVR grid using the cubic splines method (see Yurchenko et al. (2016) for details).

Only bound vibrational and rotational states were retained which meant for ^{27}AlH considering $J \leqslant 82$ for the $X\,^1\Sigma^+$ state and $J \leqslant 25$ for the $A\,^1\Pi$ state. For ^{27}AlD the range of J was increased to $J_{\rm max} = 108$ and 35, respectively. DUO input files used to generate the line lists are included as part of the supplementary data. This procedure was then simply repeated for ^{26}AlH by changing the mass of Al and nuclear statistics factor from 12 to 22. All $A\,^1\Pi$ empirical energies in the .states file of ^{27}AlH were replaced by the MARVEL values, or by values generated using PGOPHER from the constants by Szajna et al. (2015) if the MARVEL energies were not available; for ^{27}AlD we used the experimentally derived term values by Szajna et al. (2015).

The line lists are stored in the standard ExoMol format (Tennyson et al. 2016b) which involves a states file listing all the levels and a transitions file giving the Einstein A coefficients for each transition. The ^{27}AlH line list contains 1,551 states and 36 152 transitions; the ^{27}AlD line list contains 2930 states and 93 789 transitions. The ^{26}AlH line list contains 1549 states and 32 592 transitions.

Tables 2 and 3 give samples of these files. Full versions can be found at CDS, via ftp://cdsarc.u-strasbg.fr/pub/cats/J/MNRAS/, or http://cdsarc.u-strasbg.fr/viz-bin/qcat?J/MNRAS/, or from www.exomol.com.

3 RESULTS

3.1 Partition function

Partition functions were generated for each isotopologue by explicit summation of the energy levels. Comparison for ^{27}AlH with the recent results of Barklem & Collet (2016) and with the partition function generated using parameters from Sauval & Tatum (1984) shows excellent agreement for temperatures below 5000 K (see Fig. 5) once allowance is made for the fact that ExoMol adopts the HITRAN convention (Gamache et al. 2017) which includes the full nuclear spin degeneracy factor in the partition function (12 in case of ^{27}AlH, 18 in case of ^{27}AlD and 22 in case of ^{26}AlH).

It should be noted that AlH is unlikely to be important at temperatures above 5000 K.

Partition functions, $Q(T)$, on a 1 K grid up to 5000 K are given for each isotopologue in the supplementary material. For ease of use we also provide fits in the form proposed by Vidler & Tennyson (2000):

$$\log_{10} Q(T) = \sum_{n=0}^{9} a_n \left[\log T\right]^n \quad (13)$$

with the values given in Table 4.

3.2 Spectra

In the following, we present different spectra of AlH computed using the new line lists and utilizing the program EXOCROSS (Yurchenko et al. 2018a). Fig. 6 gives an overview of the AlH line list in the form of absorption cross sections for a range of temperatures from 300 to 3000 K.

Our line lists can be used to generate spectra for a variety of conditions. First we compare with available laboratory spectra. Fig. 7 compares an emission infrared spectrum of AlH recorded by White et al. (1993) with that generated using our line list assuming a temperature of 1700 K. Although the experimental spectrum does not provide an absolute intensity scale, there is good agreement for the relative intensities of the hot bands in this region between the experiment and our predictions. Our R-branch appears to be slightly stronger relative to the P-branch than the observations of White et al. (1993), but given the variable baseline and presence of self-absorption in the observed spectrum this may not be significant.

Fig. 8 shows a comparison with the emission 0–0 and 1–1 bands of the $A\,^1\Pi - X\,^1\Sigma^+$ system of AlH and AlD by Szajna et al. (2015). The observed spectrum was produced from an electric discharge in an aluminium hollow-cathode lamp. Our spectrum has been synthesized assuming a vibrational temperature of 4500 K and rotational temperature of 900 K. Comparisons with the figure suggest that the experiments had an even lower effective rotational temperature and a higher effective vibrational temperature. Inspection of Fig. 8 suggests that our 1–1 band is blue-shifted relative to the experiment by about 7 cm^{-1}. Our actual numerical agreement is much better (within experimental uncertainly), which suggest some problems with the original figure from this paper.

Fig. 9 illustrate the good agreement between our theoretical emission spectrum and the experiment of Szajna et al. (2017) for the $A\,^1\Pi - X\,^1\Sigma^+$ AlD band (1,0) at $T = 600$ K.

Rice et al. (1992) reported experimentally determined ratios of Einstein coefficients for a number of vibrational bands of $A\,^1\Pi - X\,^1\Sigma^+$, which we use to assess our transition probabilities in Table 5. Our ratios are found to be in excellent agreement with experiment.

Finally, Fig. 10 gives a comparison with the long-wavelength, rotational spectrum taken from the CDMS data base (Müller et al. 2005). The agreement between the line positions is excellent, although we recommend using the highly accurate CDMS frequency directly for long-wavelength studies of cool sources. However, there is approximately a factor of two discrepancy in the predicted line intensities. This difference is almost exactly in line with the square of the ratio of our dipole to that of Meyer & Rosmus (1975) used by CDMS. Our vibrationally averaged value for the ground state of AlH is 0.248 D, which is significantly different from the permanent μ_e value 0.158 D. We would recommend that CDMS adopts our value in future and note that using this value will approximately double the upper limit for AlH in IRC+10216 determined by Cernicharo et al. (2010).

4 CONCLUSIONS

Line lists for three AlH isotopologue species were computed using a mixture of empirical and *ab initio* curves representing our spectroscopic model. The programs DPOTFIT (Le Roy 2017a) and DUO (Yurchenko et al. 2016) were used to obtain the empirical curves, while DUO was used for the line list production. The partition functions and lifetimes were computed using the program EXOCROSS (Yurchenko et al. 2018a).

We provide comprehensive line lists for AlH isotopologue species which can be downloaded from the CDS, via ftp://cdsarc.u-strasbg.fr/pub/cats/J/MNRAS/, or http://cdsarc.u-strasbg.fr/viz-bin/qcat?J/MNRAS/, or from www.exomol.com.

ACKNOWLEDGEMENTS

We thank Nadia Milazzo and Riccardo Lanzarone for their help with the early stages of this project. This work was supported by the UK Science and Technology Research Council (STFC) No. ST/M001334/1 and the COST action MOLIM No. CM1405. This work made extensive use of UCL's Legion high-performance computing facility.

REFERENCES

Allard F., 2014, in Booth M., Matthews B. C., Graham J. R., eds. IAU Symp. 299, Exploring the Formation and Evolution of Planetary Systems. Kluwer, Dordrecht, p. 271
Baltayan P., Nedelec O., 1979, J. Chem. Phys., 70, 2399
Barklem P. S., Collet R., 2016, A&A, 588, A96
Bauschlicher C. W., Langhoff S. R., 1988, J. Chem. Phys., 89, 2116
Brown A., Wasylishen R. E., 2013, J. Mol. Spectrosc., 292, 8
Cave R. J., Johnson J. L., Anderson M. A., 1994, Intern. J. Quantum Chem., 50, 135
Cernicharo J. et al., 2010, A&A, 518, L136
Cobos C. J., 2002, J. Molec. Struct. (THEOCHEM), 581, 17
Deutsch J. L., Neil W. S., Ramsay D. A., 1987, J. Mol. Spectrosc., 125, 115
Diehl R. et al., 2003, A&A, 411, L451
Furtenbacher T., Császár A. G., 2012, J. Quant. Spectrosc. Radiat. Transf., 113, 929
Furtenbacher T., Császár A. G., Tennyson J., 2007, J. Mol. Spectrosc., 245, 115
Gamache R. R. et al., 2017, J. Quant. Spectrosc. Radiat. Transf., 203, 70
Goto M., Saito S., 1995, ApJ, 452, L147
Halfen D. T., Ziurys L. M., 2004, ApJ, 607, L63
Halfen D. T., Ziurys L. M., 2010, ApJ, 713, 520
Halfen D. T., Ziurys L. M., 2014, ApJ, 791, 65
Halfen D. T., Ziurys L. M., 2016, ApJ, 833, 89
Herbig G. H., 1956, PASP, 68, 204
Holst W., Hulthén E., 1934, Z. Phys., 90, 712
Huron B., 1969, Physica, 41, 58
Ito F., Nakanga T., Takeo H., Jones H., 1994, J. Mol. Spectrosc., 164, 379
Kaminski T. et al., 2016, A&A, 592, A42
Karthikeyan B., Rajamanickam N., Bagare S. P., 2010, Solar Phys., 264, 279
Le Roy R. J., 2007, LEVEL 8.0 A Computer Program for Solving the Radial Schrödinger Equation for Bound and Quasibound Levels. University of Waterloo Chemical Physics Research Report CP-663
Le Roy R. J., 2017a, J. Quant. Spectrosc. Radiat. Transf., 186, 179
Le Roy R. J., 2017b, J. Quant. Spectrosc. Radiat. Transf., 186, 167
Lee E. G., Seto J. Y., Hirao T., Bernath P. F., Le Roy R. J., 1999, J. Mol. Spectrosc., 194, 197
Lugaro M. et al., 2012, Meteorics Planet. Sci., 47, 1998
Mahoney W. A., Ling J. C., Wheaton W. A., Jacobson A. S., 1984, ApJ, 286, 578

Matos J. M. O., Roos B. O., Sadlej A. J., Diercksen G. H. F., 1988, Chem. Phys., 119, 71
Medvedev E. S., Meshkov V. V., Stolyarov A. V., Ushakov V. G., Gordon I. E., 2016, J. Mol. Spectrosc., 330, 36
Meyer W., Rosmus P., 1975, J. Chem. Phys., 63, 2356
Müller H. S. P., Schlöder F., Stutzki J., Winnewisser G., 2005, J. Molec. Struct. (THEOCHEM), 742, 215
Nizamov B., Dagdigian P. J., 2000, J. Chem. Phys., 113, 4124
Patrascu A. T., Hill C., Tennyson J., Yurchenko S. N., 2014, J. Chem. Phys., 141, 144312
Patrascu A. T., Tennyson J., Yurchenko S. N., 2015, MNRAS, 449, 3613
Prajapat L., Jagoda P., Lodi L., Gorman M. N., Yurchenko S. N., Tennyson J., 2017, MNRAS, 472, 3648
Rafi M., Baig M. A., Khan M. A., 1978, Nouvo Cimento Soc. Ital. Fis. B-Gen. Phys. Relativ. Astron. Math. Phys. Methods, 43, 271
Rajpurohit A. S., Reyle C., Allard F., Homeier D., Schultheis M., Bessell M. S., Robin A. C., 2013, A&A, 556, A15
Ram R. S., Bernath P. F., 1996, Appl. Optics, 35, 2879
Rice J. K., Pasternack L., Nelson H. H., 1992, Chem. Phys. Lett., 189, 43
Rivlin T., Lodi L., Yurchenko S. N., Tennyson J., Le Roy R. J., 2015, MNRAS, 451, 5153
Sauval A. J., Tatum J. B., 1984, ApJS, 56, 193
Seck C. M., Hohenstein E. G., Lien C.-Y., Stollenwerk P. R., Odom B. C., 2014, J. Mol. Spectrosc., 300, 108
Szajna W., Zachwieja M., 2009, Eur. Phys. J. D, 55, 549
Szajna W., Zachwieja M., 2010, J. Mol. Spectrosc., 260, 130
Szajna W., Zachwieja M., Hakalla R., Kepa R., 2011, Acta Phys. Pol.A, 120, 417
Szajna W., Zachwieja M., Hakalla R., , 2015, J. Mol. Spectrosc., 318, 78
Szajna W., Hakalla R., Kolek P., Zachwieja M., 2017 a, J. Quant. Spectrosc. Radiat. Transf., 187, 167
Szajna W., Moore K., Lane I. C., 2017 b, J. Quant. Spectrosc. Radiat. Transf., 196, 103
Šurkus A. A., Rakauskas R. J., Bolotin A. B., 1984, Chem. Phys. Lett., 105, 291
Tao C., Tan X. F., Dagdigian P. J., Alexander M. H., 2003, J. Chem. Phys., 118, 10477
Tennyson J., 2014, J. Mol. Spectrosc., 298, 1
Tennyson J., Yurchenko S. N., 2012, MNRAS, 425, 21
Tennyson J., Yurchenko S. N., 2017, Mol. Astrophys., 8, 1
Tennyson J., Lodi L., McKemmish L. K., Yurchenko S. N., 2016a, J. Phys. B: At. Mol. Opt. Phys., 49, 102001
Tennyson J. et al., 2016b, J. Mol. Spectrosc., 327, 73
Urban R. D., Jones H., 1992, Chem. Phys. Lett., 190, 609
Vidler M., Tennyson J., 2000, J. Chem. Phys., 113, 9766
Wallace L., Hinkle K., Livingston W., 2000, An Atlas of Sunspot Umbral Spectra in the Visible from 15 000 to 25 000 cm^{-1} (3920 to 6664 Å). Tech. Rep. Tech. Rep. 00-001, National Solar Observatory
Wells N., Lane I. C., 2011, Phys. Chem. Chem. Phys., 13, 19018
Werner H.-J., Knowles P. J., Knizia G., Manby F. R., Schütz M., 2012, WIREs Comput. Mol. Sci., 2, 242
White J. B., Dulick M., Bernath P. F., 1993, J. Chem. Phys., 99, 8371
Yamada C., Hirota E., 1992, Chem. Phys. Lett., 197, 461
Yang X., Dagdigian P. J., 1998, J. Chem. Phys., 109, 8920
Yurchenko S. N., Lodi L., Tennyson J., Stolyarov A. V., 2016, Comput. Phys. Commun., 202, 262
Yurchenko S. N., Al-Refaie A. F., Tennyson J., 2018a, A&A, 614 , A131
Yurchenko S. N., Sinden F., Lodi L., Hill C., Gorman M. N., Tennyson J., 2018b, MNRAS, 473, 5324
Zhang Y., Stuke M., 1988, Chem. Phys. Lett., 149, 310
Zhu Y. F., Shehadeh R., Grant E. R., 1992, J. Chem. Phys., 97, 883

SUPPORTING INFORMATION

Supplementary data are available at *MNRAS* online.

Please note: Oxford University Press is not responsible for the content or functionality of any supporting materials supplied by the authors. Any queries (other than missing material) should be directed to the corresponding author for the article.

This paper has been typeset from a TEX/LATEX file prepared by the author.